Published in final edited form as:
Anal Chem. 2009 January 1; 81(1): 130–138. doi:10.1021/ac801592j.

Cyclic Voltammograms at Coplanar and Shallow Recessed Microdisc Electrode Arrays: Guidelines for Design and Experiment

Jidong Guo and **Ernő Lindner***
Department of Biomedical Engineering, University of Memphis 330 Engineering Technology, Memphis, TN 38152

Abstract

Although microdisc electrode arrays (MEAs) have been extensively used for more than three decades, the existing rules do not provide an unambiguous formula for the calculation of the minimum interelectrode distance (*d*) necessary for steady state current response. With the aim of formulating generally applicable guidelines for design and experiment with MEAs, cyclic voltammograms (CVs) were simulated for coplanar and shallow recessed microdisc electrode arrays with various interelectrode distances and dimensionless scan rates (*V*). The dimensionless scan rate (*V*) is a function of the radius (*a*) of the individual electrodes in the array, the diffusion coefficient (*D*) of the analyte, and the potential scan rate (*v*). The cyclic voltammograms at microdisc electrode arrays are grouped into five categories corresponding to the contributions of linear and radial diffusion to the overall responses. These categories are illustrated in a zone diagram based on the effect of *V* and *d* on the shape of cyclic voltammograms. The zone diagram reveals the minimum *d* and a cluster of linked *d* and *V* values that are incident to sigmoidal wave responses. For shallow recessed microdisc electrode arrays, the zones representing hemispherical diffusion are larger than that for coplanar arrays. The minimum *d* necessary for hemispherical diffusion becomes smaller as recess depth increases. With the zone diagram one can predict the type of the cyclic voltammograms that can be expected for different microelectrode array geometries and experimental conditions. The fitting between simulation and experimental data validates our conclusions.

Similar to individual microelectrodes, microdisc electrode arrays have high faradaic to capacitive current ratio.[1] The magnitude of their amperometric responses is similar to macroelectrodes. Microelectrode arrays (MEAs) have shown their advantages in a variety of electroanalytical applications, e.g., end-column detection in electrophoresis,[2,3] clinical chemistry,[4,5] and environmental monitoring.[6,7,8] Since their introduction,[9] microelectrode arrays became well-accepted tools in electrophysiology[10,11] with high spatial and temporal resolution for cell and tissue studies. MEA-like behaviors are widely recognized on nanoparticles and carbon nanotube modified surfaces,[12,13,14] highly ordered pyrolytic graphite (HOPG),[15] and other graphite electrodes,[16,17] boron-doped diamond electrodes,[18] and electrodes modified with electrochemically inert membranes.[19,20] All these structures with MEA-like behavior can be considered as partially blocked electrodes[21,22,23] or electrochemically heterogeneous electrodes.[24] Microdisc electrode arrays could serve as simplified models of the real systems.

As a powerful electroanalytical method cyclic voltammetry is often the first choice to characterize a new electrochemical system. In cyclic voltammetric studies with microdisc

*To whom correspondence should be addressed. E-mail: E-mail: elindner@memphis.edu. Phone: 901-678-5641. Fax: 901-678-5281.

electrode arrays steady state responses are expected if the hemispherical diffusion layers of the individual microelectrodes are not perturbed by the diffusion layers of the neighboring microelectrodes. However, once the adjacent diffusion layers overlap, peak-shaped CVs with smaller current densities are observed. The phenomenon of overlapping diffusion layers is commonly termed as "cross-talk" or shielding effect. Obviously, if the center-to-center distance (*d*) between two adjacent microelectrodes in an array is too small or too large, the microdisc electrode array will loose its unique features and becomes similar to a macroelectrode or an individual microelectrode, respectively. Consequently the selection of an optimal microelectrode density in an array is important.

A microdisc electrode array is claimed to have steady state response[25] if

$$d>12a \tag{1}$$

where *a* is the radius of an individual electrode in the array. However, this long-standing view was proven not satisfactory by Girault.[26] Later, Davies and Compton[27] found that the much more stringent design criterion of Fletcher and Horne[28]

$$d \geq 20a \tag{2}$$

is also insufficient. To overcome the lack of generally acceptable design criteria, Davies and Compton formulated a function to calculate *d*

$$d>2\sqrt{2D\frac{\Delta E}{v}} \tag{3}$$

where ΔE is the potential range from the foot of forward wave to the reverse point and *v* is the potential scan rate. The approach of Davies and Compton is essentially different from the previous efforts because it considers several experimental parameters in determining the required minimum *d* for steady state voltammetric response. Although Davies and Compton point out that a generally applicable formula to predict *d* should contain all factors influencing the mass transport, i.e., *a, D* and *v, a* is not considered in eq.3. In the absence of a comprehensive formula simulations might be used for the accurate determination the minimum *d* in a microelectrode array.[28] The absence of theory-based general guidelines for microelectrode array design impelled experimental optimization attempts.[29,30]

Most previous theoretical studies focused on finding a *d* value which is sufficiently large to exclude the possibility of diffusion layer overlapping. But the zone diagram of Amatore et.al. [21] reveals that regardless of the size of *d* there will be cross-talk between adjacent individual microelectrodes at certain scan rates because the diffusion layer at disc electrodes continuously enlarge with the square root of time.[31] In other words, in a quiescent solution no sufficiently large *d* exists that could prevent the overlap of the diffusion layers over the individual microelectrodes in the array at all possible potential scan rates. Consequently, the design guidelines for microdisc arrays should rather provide a necessary *d* which is large enough to allow the development of hemispherical diffusion layers over the individual microelectrodes in the array in a window of potential scan rates. General guidelines for designing microdisc electrode arrays could avoid lengthy and expensive experimental optimization.

The diffusion layer evolving over a microdisc electrode array in cyclic voltammetric experiments depends on *d, a, v* and *D*. The difficulty in formulating a universal expression for

d can be reduced by using dimensionless parameters, most importantly the dimensionless scan rate *V* instead of three independent parameters *a, v* and *D*: [32]

$$V=\frac{nF}{4RT}\cdot\frac{va^2}{D} \tag{4}$$

where *n* is the number of electrons transferred in the electrode reaction, *F* is the Faraday constant, *R* is the universal gas constant and *T* is the thermodynamic temperature. Although similar dimensionless scan rate has been used in theoretical studies of cyclic voltammetry at MEA, its power to simplify this particular problem and the possibility of utilizing it for formulating general guidelines for the design and experiments was overlooked.[22,33]

In this paper, the effect of *V* and *d* on the shape of CVs recorded with coplanar microelectrode arrays is presented in a zone diagram which reveals the necessary *d* for sigmoidal response. MEAs are most commonly fabricated with photolithographic techniques. This fabrication process generally provides MEAs that are slightly recessed.[34] To show the consequences of this MEA geometry compared to coplanar MEAs the cyclic voltametric behavior of shallow recessed microdisc electrode arrays were simulated and the necessary *d* for sigmoidal response was determined.

THEORY

Model for a Coplanar Infinite Microdisc Electrode Array in Hexagonal Lattice

A hexagonally arranged microdisc array is shown in Figure 1a, where the repeating unit is illustrated by the mesh-filled triangle. The simulation of the voltammetric response of a coplanar microdisc array is a 3-dimensional problem. Although commercially available finite element softwares have been used to solve similar 3-dimensional problems,[26,35] the 3-dimensional simulation is unappealing if a 2-dimensional approximation can provide satisfactory results. The 2-dimensional simulation is indeed a widely accepted approach [21, 28,36,37] which is especially attractive when a large number of simulations must be performed. The accuracy of the 2-dimensional simulation compared to 3-dimensional simulation can be found in the Supporting Information.

The 2-dimensional simulation takes some assumptions. In brief, each microelectrode can be assigned its own hexagon as shown in Figure 1a. The net fluxes passing through the boundaries of hexagons are zero in voltammetric experiments. These hexagons are replaced by equal-area circles with radius R_0, like the mesh-filled circle in Figure 1a. The cylindrical symmetry of this unit cell simplifies the simulation to a 2-dimensional problem in which only the plane shown in the left panel of Figrue 1b needs to be considered. The same idea can also be applied to recessed microdisc electrode arrays with a recess depth *l* (Figure 1b, right panel)

To simulate the cyclic voltammetric response, a fast one-electron transfer reaction with Bulter-Volmer kinetics is considered

$$\mathrm{O}+e^-\underset{k_b}{\overset{k_f}{\rightleftharpoons}}\mathrm{R} \tag{5}$$

The forward and backward rate constants, k_f and k_b, are defined by

$$k_f=k^0\exp\left(-\frac{\alpha F}{RT}(E-E^{0\prime})\right) \tag{6}$$

$$k_b=k^0\exp(-\frac{(1-\alpha)F}{RT}(E-E^{0\prime})) \tag{7}$$

where k^0 is the standard heterogeneous rate constant for the redox couple, α is the transfer coefficient (α = 0.5 is taken in this work), $E^{0'}$ is the formal potential, E is the applied potential on the electrode/solution interface. The diffusion of species O and R in the solution can be expressed as

$$\frac{\partial c_o(r,z,t)}{\partial t}=D_o\left[\frac{\partial^2 c_o(r,z,t)}{\partial r^2}+\frac{1}{r}\frac{\partial c_o(r,z,t)}{\partial r}+\frac{\partial^2 c_o(r,z,t)}{\partial z^2}\right] \tag{8}$$

$$\frac{\partial c_R(r,z,t)}{\partial t}=D_R\left[\frac{\partial^2 c_R(r,z,t)}{\partial r^2}+\frac{1}{r}\frac{\partial c_R(r,z,t)}{\partial r}+\frac{\partial^2 c_R(r,z,t)}{\partial z^2}\right] \tag{9}$$

where the c_O, c_R, D_O and D_R are the concentrations and diffusion coefficients of respective species. Before the experiment starts, only the species O is present in the solution with initial bulk concentration of c_b. If we take the common assumption of $D_O = D_R$, then $c_R = c_b - c_O$ applies to the entire simulation domain. The initial conditions for coplanar and recessed microelectrode arrays are given as

$$c_o=c_b \quad 0\le r\le R_0, 0\le z\le z_{max} \tag{10}$$

$$c_R=0 \quad 0\le r\le R_0, 0\le z\le z_{max} \tag{11}$$

where $R_0=\sqrt{\frac{\sqrt{3}}{2\pi}}d$, z_{max} is the maximum z value in the simulation domain which is far from the outer boundary of the diffusion layer. The boundary conditions for a coplanar microdisc electrode array (Figure 1b left panel) are:

$$D_o\left[\frac{\partial c_o(r,z,t)}{\partial z}\right]_{z=0}=-D_R\left[\frac{\partial c_R(r,z,t)}{\partial z}\right]_{z=0}=k_f c_o(r,z,t)-k_b c_R(r,z,t) \tag{12}$$

$$D_o\left[\frac{\partial c_o(r,z,t)}{\partial r}\right]_{r=0}=D_R\left[\frac{\partial c_R(r,z,t)}{\partial r}\right]_{r=0}=0 \quad 0<z<z_{max} \tag{13}$$

$$D_o\left[\frac{\partial c_o(r,z,t)}{\partial r}\right]_{r=R_0}=D_R\left[\frac{\partial c_R(r,z,t)}{\partial r}\right]_{r=R_0}=0 \quad 0<z<z_{max} \tag{14}$$

$$D_{\mathrm{O}}\left[\frac{\partial c_{\mathrm{O}}(r,z,t)}{\partial z}\right]_{z=0}=D_{\mathrm{R}}\left[\frac{\partial c_{\mathrm{R}}(r,z,t)}{\partial z}\right]_{z=0}=0 \quad a<r<R_0 \tag{15}$$

$$c_{\mathrm{O}}=c_b \quad z=z_{\max},0<r<R_0 \tag{16}$$

$$c_{\mathrm{R}}=0 \quad z=z_{\max},0<r<R_0 \tag{17}$$

For a recessed microdisc electrode array, shown in the right panel of Figure 1b, the boundary conditions are

$$D_{\mathrm{O}}\left[\frac{\partial c_{\mathrm{O}}(r,z,t)}{\partial z}\right]_{z=-l}=-D_{\mathrm{R}}\left[\frac{\partial c_{\mathrm{R}}(r,z,t)}{\partial z}\right]_{z=-l}=k_{\mathrm{f}}c_{\mathrm{O}}(r,z,t)-k_{\mathrm{b}}c_{\mathrm{R}}(r,z,t) \tag{18}$$

$$D_{\mathrm{O}}\left[\frac{\partial c_{\mathrm{O}}(r,z,t)}{\partial r}\right]_{r=0}=D_{\mathrm{R}}\left[\frac{\partial c_{\mathrm{R}}(r,z,t)}{\partial r}\right]_{r=0}=0 \quad -l<z<z_{\max} \tag{19}$$

$$D_{\mathrm{O}}\left[\frac{\partial c_{\mathrm{O}}(r,z,t)}{\partial r}\right]_{r=a}=D_{\mathrm{R}}\left[\frac{\partial c_{\mathrm{R}}(r,z,t)}{\partial r}\right]_{r=a}=0 \quad -l<z<0 \tag{20}$$

and eqs 14 to 17 also apply.

The time scale (t_{c}) of the cyclic voltammetric experiment is

$$t_{\mathrm{c}}=\frac{2(E_{\mathrm{i}}-E_r)}{v} \tag{21}$$

where E_{i} is the initial potential, E_{r} is the reversal potential in cyclic voltammetry. The triangle wave of *E*-*t* in cyclic voltammetry can be expressed as

$$E=E_{\mathrm{i}}+(E_{\mathrm{r}}-E_{\mathrm{i}})\cdot\frac{2}{\pi}\sin^{-1}\left\{\sin\left[\frac{\pi vt}{2(E_{\mathrm{r}}-E_{\mathrm{i}})}\right]\right\} \quad 0\le t\le t_{\mathrm{c}} \tag{22}$$

The current passing through the individual microelectrode/solution interfaces can be calculated by

$$i=2\pi\mathrm{F}D_{\mathrm{O}}\int_0^a r\left[\frac{\partial c_{\mathrm{O}}(r,z,t)}{\partial z}\right]_{z=0}dr \tag{23}$$

for coplanar microdisc electrode arrays and

$$i=2\pi \mathrm{FD_o}\int_0^a r\left[\frac{\partial c_\mathrm{o}(r,z,t)}{\partial z}\right]_{z=-l} dr \quad (24)$$

for recessed microdisc electrode arrays.

The time-dependent diffusion problems defined above were solved by a COMSOL Multiphysics® version 3.2 (COMSOL, Inc., Burlington, MA, USA) program, which applies the finite element method. For a general treatment the following dimensionless parameters were used:

$$C_\mathrm{o}=c_o/c_0 \quad (25)$$

$$C_\mathrm{R}=c_R/c_0 \quad (26)$$

$$R=r/a \quad (27)$$

$$Z=z/a \quad (28)$$

$$L=l/a \quad (29)$$

$$K_0=\frac{k_0 a}{D} \quad (30)$$

$$\varepsilon=\frac{n\mathrm{FE}}{RT} \quad (31)$$

$$\tau=\frac{4Dt}{a^2} \quad (32)$$

The dimensionless scan rate, V, has been described in eq 4. Simulation of each CV took between 5 and 10 minutes on a PC equipped with a Pentium D 3.4 GHz processor, 4 GB memory, and Windows XP Professional Edition operating system.

Zone Diagram of Cyclic Voltammetry at Coplanar Microelectrode Array

The diffusion over the MEA can be classified as five categories. These categories are shown schematically in Figure 2: (I) planar diffusion layer over the individual microelectrodes; (II) mixed diffusion layers over individual microelectrodes, i.e., transition between planar and hemispherical diffusion layers; (III) hemispherical diffusion layers over the individual

microelectrodes; (IV) mixed diffusion layer due to overlapping of the individual diffusion layers; (V) planar diffusion layer over the entire microelectrode array. Category I and II were not distinguished before.

To have a quantitative definition of these categories simulations have been performed to reveal the correlation between d and V, and to determine the dominating mode of diffusion in cyclic voltammetric experiments with MEAs under different experimental conditions (v, D). These simulations were also aimed to provide generally applicable guidelines for MEA design (d, a) and experiment (v, D). The simulations have been performed at a variety of dimensionless scan rates (V) at selected d values ranging between $d = 2.3a$ and $d = 200a$. With these simulations the borders between the diffusion categories could be formulated as dimensionless transition scan rates using the criteria formulated in Table 1. These dimensionless transition scan rates, i.e., $V12$, $V23$, $V34$ and $V45$ represent the borderlines between the diffusion modes I and II, II and III, III and IV (II and IV in certain domain), IV and V, respectively as shown in Fig. 2. The results of these simulations also provided a V vs. d plot, a zone diagram, in which both V and d are plotted on logarithmic scales (Figure 3). The expressions for the borderlines between different diffusion categories are listed in Table 2. The symbols and acronyms used to define the borderlines in the zone diagram are included in the list of symbols (Table 3).

The $V12$, $V23$, $V34$ and $V45$ border lines divide the V vs. d diagram into zones labeled with roman numbers. Zones I through V represent the diffusion categories of Figure 2. For example the CVs grouped into zone I, the area above the $V12$ line, are fully planar diffusion dominated with no overlap of the diffusion layers of the individual electrodes in an array. Similarly, zone II in Figure 3 correspond to category II in Figure 2. Zone II is bordered by the $V12$, $V23$ and the $V34$ lines. The CVs in this zone are in a mix diffusion mode with contribution from linear and radial diffusion. Note that in this zone the CVs of the individual microelectrodes in an array are same as the CVs of a single microelectrode. Zone III in Figure 3 correspond to category III in Figure 2. It is defined as the area in between $V23$ and $V34$ lines. Zone III has unique importance because sigmoidal voltammetric responses can only be achieved in cyclic voltammetric experiments with MEAs if their design (d, a) and the applied experimental conditions (v, D) correspond to the criteria of zone III. The intersection of the $V23$ and $V34$ borderlines of zone III is at $d = 23.0a$. This intersection defines $d = 23.0a$ as a universally applicable necessary center-to-center distance ($d_{necessary}$) in coplanar microdisc electrode array design that is required for recording sigmoidal voltammetric responses. However, from the zone diagram it is obvious that the selection of a slightly larger value than the $d_{necessary}$, e.g., $d = 24a$, is not sufficient for a steady state response. Indeed the CVs of MEAs with $d = 24a$ can fall in all of the zones depending on the applied V. To achieve sigmoidal response requires the careful selection of a combination of a and v values (with given D) to make the dimensionless scan rate fall in the narrow gap between the $V34$ and $V23$ lines at $d = 24a$, i.e., $V = 0.07$ and $V = 0.08562$, respectively. It is essential to recognize that between $d = 2.3a$ and $d = 200a$ there is no such a center-to-center distance at which all V is incident to steady state voltammograms. For this reason, it should be noted that there is no real “steady state” at microdics electrode array in a quiescent solution. Even the CV recorded with an array with interelectrode distance of $200a$ can show notable deviation from sigmoidal wave once the dimensionless scan rate is below 9.341×10^{-6}. This dimensionless scan rate can be generated for example by the combination of $a = 50$ nm and $v = 0.384$ V/s or $a = 100$ nm and $v = 0.096$ V/s, given $D = 10^{-5}$ cm^2/s. Consequently, the CVs of nanoelectrode arrays recorded at commonly applied scan rates (e.g., 0.02 V/s or 0.05 V/s) can easily fall into zone IV (partial linear and partial radial diffusion mode), even if they were manufactured with extremely large center-to-center distances between individual electrodes. The information provided by this diagram is expected to be useful in designing nanoelectrode arrays and nanoelectrode ensembles,[38,39,40] and in selecting the most adequate experimental conditions in their applications.[41]

CVs grouped into category IV in Figure 2, related to their partial linear and partial radial diffusion, can fall into zones IV and VI in Figure 3. Zones IV and VI are virtually separated by the extension of the *V*23 borderline indicating that the dense packed arrays leaves no possibility to sigmoidal voltammetric response because the overlapping of diffusion layers occurs in shorter time then needed for achieving hemispherical diffusion layer. CVs in zones V correspond to category V behavior in Figure 2 where planar diffusion layer spreads over the entire surface of an electrode array.

The borderlines of Figure 3, *V*12, *V*23, *V*34 and *V*45 were defined as the boundaries between categories I through V. These boundaries were quantified with current criteria and a subjectively selected level of deviation (5%) from the shape of "standard" CVs. The "standard" CVs were defined as ones solely linear diffusion controlled ($V = 7789$ at single inlaid microdisc electrode) or solely hemispherical diffusion controlled ($V = 10^{-6}$ at single inlaid microdisc electrode). The shape deviation was assessed by comparing γ ($\gamma = I_{max,\ reverse}/I_{max,\ forward}$) values of a CV to a criterion given in Table 1, where γ_{linear} is the ratio of $I_{max,\ reverse}$ to $I_{max,\ forward}$ in a fully linear diffusion controlled CV. Finding the points on line *V*34 and line *V*45 above line *V*23 is less trivial. The points on the section of the *V*34 line, below the *V*23 line, represent CVs with maximum currents on individual discs ($I_{max,\ individual}$) less than the steady state current on single disc ($I_{ss,\ single}$) and shapes which are 5% different from the ideal sigmoidal shape. The points on line *V*34, above line *V*23, were determined by finding dimensionless scan rates which would generate CVs with lower maximum current on individual discs than it could be expected for a single electrode ($I_{max,\ single}$) and with 5% increased γ compared to the value expected for a single electrode at the same *V* (γ_{single}). This pair by pair comparison with single electrode CVs was necessary because above the *V*23 line the shapes of the CVs contain both linear and radial diffusion component. The simpler current and shape comparisons for the lower part of *V*34 are possible because all CVs with $V \leq V23$ are sigmoidal waves at single electrode. The criteria for the maximum current quantify the diffusion layer overlapping while the criteria for γ measure the tolerance of deviation. In summary, the line *V*34 separates two kinds of CV behaviors at microelectrode arrays with 5% tolerance: (1) the individual discs in an array behave like independent microelectrodes when a particular *V* and *d* combination places the CV above the *V*34 line, which can be peak-shaped CVs and sigmoidal CVs; (2) the current responses of the individual microelectrodes in an array are influenced by significant overlapping of the individual diffusion layers when a selected *V* and *d* combination places the CVs below the *V*34 line. Similar to the above, the points on the section of the *V*45 line above *V*23 line were determined by finding dimensionless scan rates which would generate CVs for the individual discs with lower maximum current than it could be expected for a single electrode and with 5% smaller γ compared with a fully planar diffusion dominated CV.

Line *V*12 and *V*45 intersect at $d = 2.16a$. If an infinite microdisc electrode array is packed with microelectrode sites denser than this limit, the CVs recorded with such arrays will be always fully planar diffusion dominated at any *v* and *a* combination in a quiescent solution. However, once *d* becomes larger than $2.16a$ the shapes of MEA CVs will change with the dimensionless scan rate indicating a patterned surface with electrochemically active (electrode) and inactive (insulated) areas. With *d* smaller than $2.16a$ eventual patterns on an electrode surface will not influence the CVs, i.e., the microelectrode array will always behave as a macroelectrode with electrochemically homogeneous surface. Some graphite electrodes[30] and nanoparticles[42] or carbon nanotube modified electrodes may drop in this special category.

Although the zone diagram of Figure 3 is based on the simulations reflecting the geometrical conditions of hexagonally arranged microdisc electrode arrays, its significance can be generalized for other type of microelectrode arrays or microelectrode ensembles by changing the *x*-axis from the center to center distance (*d*) to the fractional area of the microelectrodes in

an array (θ), i.e., to the ratio of the active (electrode) vs. inactive (insulator) areas in a MEAs. For the hexagonal arrangement of electrodes in an MEA θ becomes:

$$\theta = \frac{2\pi a^2}{\sqrt{3}d^2} \tag{33}$$

The zone diagram simplifies to a line diagram of V if it is applied to single microelectrodes. This line is separated into 3 segments by points corresponding to the $V12$ and $V23$ lines in the zone diagram. With the help of these $V12$ and $V23$ points the modes of mass transport in cyclic voltammetric experiments can be quantitatively categorized for any given v, a and D as: (I) planar diffusion controlled, (II) mixed linear and radial diffusion controlled, and (III) solely hemispherical diffusion controlled. These categories are reflected in the shape of the single microelectrode CVs. The $V34$ and $V45$ lines have no relevance for single microelectrodes.

It has been demonstrated that the V vs. d zone diagram is adequate for selecting a combination of microdisc electrode array design and experimental parameters for a desired behavior in cyclic voltammetric experiments, or for predicting the shape of voltammograms of MEAs or single microelectrodes if the geometrical parameters and the experimental conditions are known. Based on Amatore's zone diagram[21], one can predict the shapes of the CVs which belong in Zones III, IV and V. But CVs belonging in Zones I, II, VI and the line $V23$ were not included in the zone diagram of Amatore et. al. But Zone II and the $V23$ line are actually very important in the determination of the necessary d for attaining sigmoidal voltammetric response with a MEA. Indeed, the intersection of the $V23$ and $V34$ lines determines $d_{necessary}$. Without unambiguous dimensionless transition scan rates separating the mixed diffusion zones (Zone II and IV) and the hemispherical diffusion zone (Zone III) it is impossible to formulate an eloquent answer for $d_{necessary}$. Since the motivation for the zone diagram presented in this work has been to provide convenient guidelines for MEA design and for selecting adequate experimental conditions in experiments with MEAs, the zone diagram has been devised with this intent by employing the dimensionless scan rate and interelectrode distance.

The necessary interelectrode distance ($d_{necessary}$) for Shallow Recessed Microdisc Electrode Arrays

Microdisc electrode arrays fabricated by thin film photolithography are normally shallow recessed.[34] To provide accurate zone diagram for this class of MEAs we extended our study to shallow recessed microdisc electrode arrays. As emphasized above, the location of the $V23$ line has fundamental importance in the determination of $d_{necessary}$. The position of the $V23$ line changes simultaneously with changes in the recess depth (L). Interestingly, as L changes from 0 to 30, $V23$ passes a maximum at ca. $L = 0.75$.[43] Similarly, as shown in Fig. 4, the position of the $V34$ line changes with changing L. Indeed, the $V34$ line descends as L increases, reflecting the increased diffusion times in the well. On the other hand, for $0 < L \leq 2$, the value of $V23$ is larger than the value of $V23$ at $L = 0$ (0.08562). Consequently, due to the oppositely changing trends of $V23$ and $V34$ lines in this recess depth range, the area of Zone III for recessed well MEAs is larger compared to coplanar microdisc electrode arrays. In Figure 4 the intersections labeled for the different L values are $V23$ / $V34$ line intersections which define the $d_{necessary}$ values for L= 0, 0.2, 0.75, 2, 5, respectively. As shown in Fig. 5, $d_{necessary}$ gradually decreases as L increases (Figure 5). For $L < 0.75$, this decrease is a consequence of the shifts in $V23$ and $V34$ lines. But for $L > 0.75$ values the decrease is controlled by the shift in the $V34$ position. The plot of $d_{necessary}$ vs. L, in the range of $0 \leq L \leq 5$, was fitted to an exponential decay function for the convenience of application for shallow recessed microdisc electrode array.

$$d_{\text{necessary}} = 10.86 + 6.218\exp\left(-\frac{L+0.0888}{0.222}\right) + 9.435\exp\left(-\frac{L+0.0888}{0.492}\right) \quad (34)$$

To find dimentionless scan rate range in which sigmoidal CVs can be expected with shallow recessed microdisc electrode arrays with given d and L, one can either use corresponding $V23$ and $V34$ as upper and lower limit, or take $V34$ for coplanar MEA as a conservative estimate for the lower limit.

EXPERIMENTAL SECTION

Chemicals

Ferrocenemethonal (97%) was obtained from Sigma-Aldrich (St. Louis, MO). Other chemicals were reagent grade and were used as received from commercial sources. All aqueous solutions were prepared with 18.2 MΩ · cm^{-1} deionized water (Nanopure, Barnstead, Dubuque, IA)

Electrodes and Electrochemical Measurments

The hexagonally arranged gold microdisc arrays were fabricated by Aegis Technologies Group, Inc. (Huntsville, AL) on glass substrate using standard thin film photolithography. The individual gold disc electrodes of a = 5 μm and l = 1 μm were patterned with d = 100 μm or 150 μm interelectrode distances over a 3 mm diameter circular area using polyimide as insulating material.

Cyclic voltammetric experiments were performed with a CHI 760C electrochemical workstation (CH Instruments, Austin, TX). In the three-electrode setup a Ag/AgCl reference electrode (CH Instruments, Austin, TX), and a Pt wire counter electrode were used in combination with one of the Pt microelectrodes or a microelectrode array as working electrode.

RESULTS AND DISCUSSION

Fitting with experimental results at Recessed Microdisc Electrode Arrays

The individual microdisc electrodes in the MEAs used in our experiments are formed on the bottom of slightly recessed wells with 1 μm depth. These interconnected microelectrode arrays[8,34] are made by patterning hexagonally arranged circular openings by standard photolithography into a 1 μm thick polyimide insulation layer over a large gold disc electrode. With a scan rate of 0.05 V/s, the simulated CV for $d = 30a$, $l = 0.2a$ and $D = 7.4 \times 10^{-6}$ cm^2/s for ferrocenemethanol[44] shows excellent agreement both on the forward and reverse scans with experimental data obtained with an array of a = 5 μm, d = 150 μm and l = 1.0 μm (Figure 6a). The comparison of the simulated curves of the coplanar and the recessed MEAs shows that the linear diffusion contribution is somewhat larger at the coplanar microelectrode array, and this is consistent with what we observed at single shallow recessed microdisc electrode.[43] The value of γ in the CV of coplanar MEA slightly exceeds the 5% tolerance, labeled as a dotted horizontal line in Figure 6a, while the value of γ in the CV of recessed MEA is less than 5%. Apparently, the recessed electrode geometry obstructs the expansion of the diffusion layer towards to the wall of the diffusion domain and delays the overlapping of the adjacent diffusion layers. These results show that the experimental value of $V34$ for recessed microelectrode arrays, with $d = 30a$ and $l = 0.2a$, is lower than 0.01644 (v = 0.05 V/s and a = 5 μm with $D = 7.4 \times 10^{-6}$ cm^2/s for ferrocenemethanol in Figure 6a), while the value of $V34$ for a coplanar array with $d = 30a$ is 0.02335. The value of $V34$ for $d = 30a$ and L = 0.2 from Figure 4 is determined as 0.01167 (v = 0.035 V/s with the same a and D) from Figure 4. Experimental CVs in Figure 6a belong in zone III.

Figure 5 predicts that $d_{necessary}$ is smaller on a recessed microdisc electrode array compared with coplanar array. Our experiments at MEA with $d = 20a$ and $L = 0.2$ supports this expectation. The $d_{necessary}$ for coplanar microdisc electrode array is 23.0, but as shown in Figure 6b, a practically sigmoidal wave was observed at the recessed microelectrode array with a = 5 μm, d = 100 μm and l = 1 μm at v = 0.2 V/s. From Figure 5, the $d_{necessary}$ for recessed microdisc electrode array with $L = 0.2$ is 17.84. The simulated curve for recessed array is also in almost perfect agreement with the experimental CV (Figure 6b). The γ values for the computed and experimental CVs of Figure 6b were almost exactly at the 5% deviation line. The γ values for the simulated CV of coplanar arrays exceed the 5 % limit. As shown in Figure 6c, at a scan rate of 0.02 V/s ($V = 0.006574$) the effect of overlapping diffusion layers becomes apparent on the CVs at the same recessed MEAs. With increasing overlapping of the diffusion layers the difference in the shape of the CVs of the recessed and the coplanar microelectrode arrays becomes more significant (Figure 6c).

It is important to emphasize that the simulations in this account were performed for microelectrode arrays of infinite extension. It means that the somewhat different contribution of microelectrodes located at the edge of the array to the total current has not been considered. Three-dimensional simulations (data not shown) demonstrate that if considerable overlapping of the diffusion layers influences the MEA responses then besides the microelectrodes at the very edge[26] of the array, microelectrodes close to the edge of the array also present higher currents and less linear diffusion contribution in comparison to the central microelectrodes, especially for densely packed arrays. This makes the consideration of a finite MEA size (the edge effect) in simulations rather complicated. However, the interference related to the limited size of an array is negligible when the CVs are categorized as category I, II, III (Figure 2) because in these categories the individual microelectrodes in the arrays behave like single microelectrodes, i.e., their contribution to the total current is independent from their location in the array. The effect of the different current responses of microelectrodes at the edge of the array is also insignificant when the overlapping of the diffusion layers between the individual microelectrodes in the array is not very severe, e.g., in zone IV close to the $V34$ borderline. But in zone IV besides the area close to line $V34$, and in zones V and VI, the difference between infinite and finite arrays is not negligible. As a special case of finite microdisc arrays, when the dimension of the array drops in the microelectrode range, e.g. nanoelectrode arrays in micron size, [40,44] the diffusion layers over the entire array will be hemispherical for Zone V.

CONCLUSIONS

Cyclic voltammograms of coplanar and recessed microdisc electrode arrays have been simulated to categorize their voltammetric behavior. The behavior of MEAs in cyclic voltammetric experiments has been grouped into five main categories in a quantitative way based on the contribution of linear and radial diffusion to the overall current responses. These categories are illustrated in a zone diagram based on the effect of the dimensionless scan rate (V) and the center-to-center distance between electrodes (d) on the shape of cyclic voltammograms. The boundaries between the zones, were revealed by numeric simulations, and validated by experimental data. The intersection of two borderlines between mixed diffusion and hemispherical diffusion provides the necessary d which is required for sigmoidal wave in cyclic voltammetric experiments.

The zone diagram provides a generally applicable, unambiguous guideline for microelectrode array design. It shows that coplanar MEAs of $d \geq 23a$ are expected to present sigmoidal wave only if the experimental scan rate falls into a certain scan rate range. The area of the zone in which sigmoidal CVs can be expected is larger for shallow recessed arrays in the zone diagram. For recessed microdisc electrode arrays, $d_{necessary}$ were determined for $0 < L < 5$. Using the

zone diagram one can also predict the voltammetric behavior of microdisc electrode array if the design parameters of the array and the experimental conditions are known.

Supplementary Material

Refer to Web version on PubMed Central for supplementary material.

ACKNOWLEDGEMENT

The authors thank the financial support of the NIH/NHLBI #1 RO1 HL079147 grant.

REFERENCE

1. Amatore, C. Physical Electrochemistry: Principles, Methods and Applications. Rubenstein, I., editor. New York: Marcel Dekker; 1995. p. 131
2. Liu J, Zhou WH, You TY, Li FL, Wang EK, Dong SJ. Anal. Chem 1996;68:3350–3353.
3. Kappes T, Hauser PC. Electroanalysis 2000;12:165–170.
4. Zhang SQ, Zhao HJ, John R. Anal. Chim. Acta 2000;421:175–187.
5. Albers J, Grunwald T, Nebling E, Piechotta G, Hintsche R. Anal. Bioanal. Chem 2003;377:521–527. [PubMed: 14504676]
6. Belmont C, Tercier ML, Buffle J, Fiaccabrino GC, Koudelka-Hep M. Anal. Chim. Acta 1996;329:203–214.
7. Feeney R, Kounaves SP. Anal. Chem 2000;72:2222–2228. [PubMed: 10845367]
8. Feeney R, Kounaves SP. Electroanalysis 2000;12:677–684.
9. Thomas DA, Springer PA, Loeb GE, Berwald-Netter Y, Okun LM. Exp. Cell Res 1972;74:61–66. [PubMed: 4672477]
10. Maher MP, Pine J, Wright J, Tai YC. J. Neurosci. Meth 1999;87:45–56.
11. Stett A, Egert U, Guenther E, Hofmann F, Meyer T, Nisch W, Haemmerle H. Anal. Bioanal. Chem 2003;377:486–495. [PubMed: 12923608]
12. Dai X, Wildgoose GG, Salter C, Crossley A, Compton RG. Anal. Chem 2006;78:6102–6108. [PubMed: 16944890]
13. Welch CW, Compton RG. Anal. Bioanal. Chem 2006;384:601–619. [PubMed: 16402180]
14. Wilson NR, Guille M, Dumitrescu I, Fernandez VR, Rudd NC, Williams CG, Unwin PR, Macpherson JV. Anal. Chem 2006;78:7006–7015. [PubMed: 17007527]
15. Banks CE, Davies TJ, Wildgoose GG, Compton RG. Chem .Comm 2005;7:829–841. [PubMed: 15700054]
16. Davies TJ, Moore RR, Banks CE, Compton RG. J. Electroanal. Chem 2004;574:123–152.
17. Davies TJ, Hyde ME, Compton RG. Angew. Chem. Int. Ed 2005;44:5121.
18. Holt KB, Bard AJ, Show Y, Swain GM. J. Phys. Chem. B 2004;108:15117–15127.
19. Sabatani E, Rubinstein I. J. Phys. Chem 1987;91:6663–6669.
20. Jeoung E, Galow TH, Schotter J, Bal M, Ursache A, Tuominen MT, Stafford CM, Russell TP, Rotello VM. Langmuir 2001;17:6396–6398.
21. Amatore C, Savéant JM, Tessier D. J. Electroanal. Chem 1983;147:39–51.
22. Brooks BA, Davies TJ, Fisher AC, Evans RG, Wilkins SJ, Yunus K, Wadhawan JD, Compton RG. J. Phys. Chem. B 2003;107:1616–1627.
23. Davies TJ, Brooks BA, Fisher AC, Yunus K, Wilkins SJ, Greene PR, Wadhawan JD, Compton RG. J. Phys. Chem. B 2003;107:6431–6444.
24. Davies TJ, Banks CE, Compton RG. J Solid State Electrochem 2005;9:797–808.
25. Saito Y. Rev. Polarogr 1968;15:177–187.
26. Lee HJ, Beriet C, Ferrigno R, Girault HH. J. Electroanal. Chem 2001;502:138–145.
27. Davies TJ, Compton RG. J. Electroanal. Chem 2005;585:63–82.
28. Fletcher S, Horne MD. Electrochem. Commun 1999;1:502–512.

29. Seddon BJ, Shao Y, Girault HH. Electrochim Acta 1994;39:2377–2386.
30. Sandison ME, Anicet N, Glidle A, Cooper JM. Anal. Chem 2002;74:5717–5725. [PubMed: 12463354]
31. Amatore C, Fosset B. Anal. Chem 1996;68:4377–4388.
32. Rodgers PJ, Amemiya S. Anal. Chem 2007;79:9276–9285. [PubMed: 18004818]
33. Chevallier FG, Jiang L, Jones TGJ, Compton RG. J. Electroanal. Chem 2006;587:254–262.
34. Fiaccabrino GC, Koudelka-Hep M. Electroanalysis 1998;10:217–222.
35. Beriet C, Ferrigno R, Girault HH. J. Electroanal. Chem 2000;486:56–64.
36. Gueshi T, Tokuda K, Matsuda H. J. Electroanal. Chem 1978;89:247–260.
37. Shoup D, Szabo A. J. Electroanal. Chem 1984;160:19–26.
38. Arrigan DWM. Analyst 2004;129:1157–1165. [PubMed: 15565213]
39. Menon VP, Martin CR. Anal. Chem 1995;67:1920–1928.
40. Zoski CG, Yang N, He P, Berdondini L, Koudelka-Hep M. Anal. Chem 2007;79:1474–1484. [PubMed: 17297946]
41. Baker WS, Crooks RM. J. Phys. Chem 1998;102:10041–10046.
42. Cheng W, Dong S, Wang E. Anal. Chem 2002;74:3599–3604. [PubMed: 12175142]
43. Guo J, Lindner E. J. Electroanal. Chem. 2008 Sept 3;Submitted
44. Guo J, Amemiya S. Anal. Chem 2005;77:2147–2156. [PubMed: 15801749]

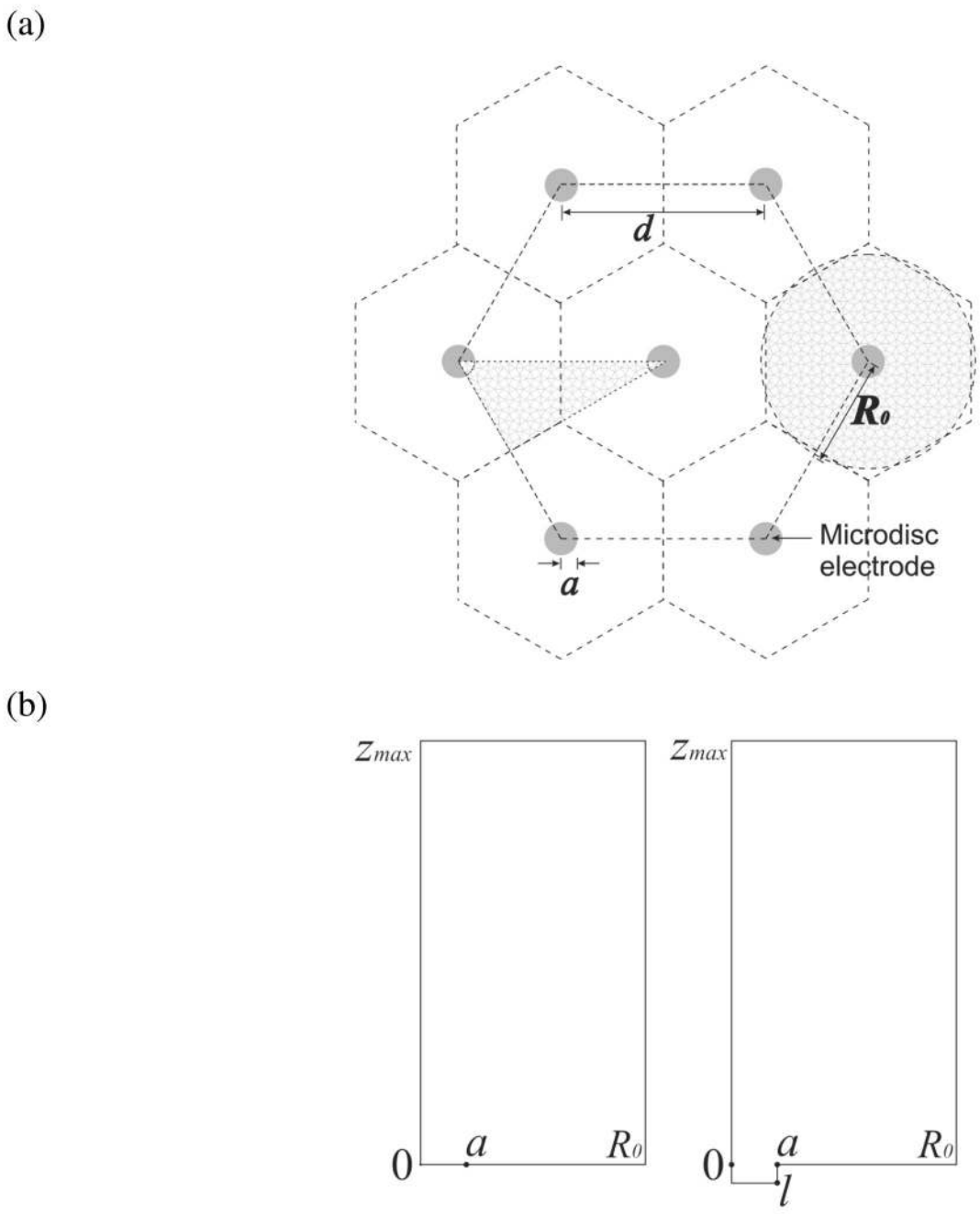

Figure 1.
Hexagonal mirodisc electrode array and the conditions for the diffusion domain approach. (a) microdisc array with hexagonal arrangement, insulator is in white; (b) space domains defined for a finite element simulation of cyclic voltammetry at coplanar (left) and recessed (right) regular microdisc electrode arrays.

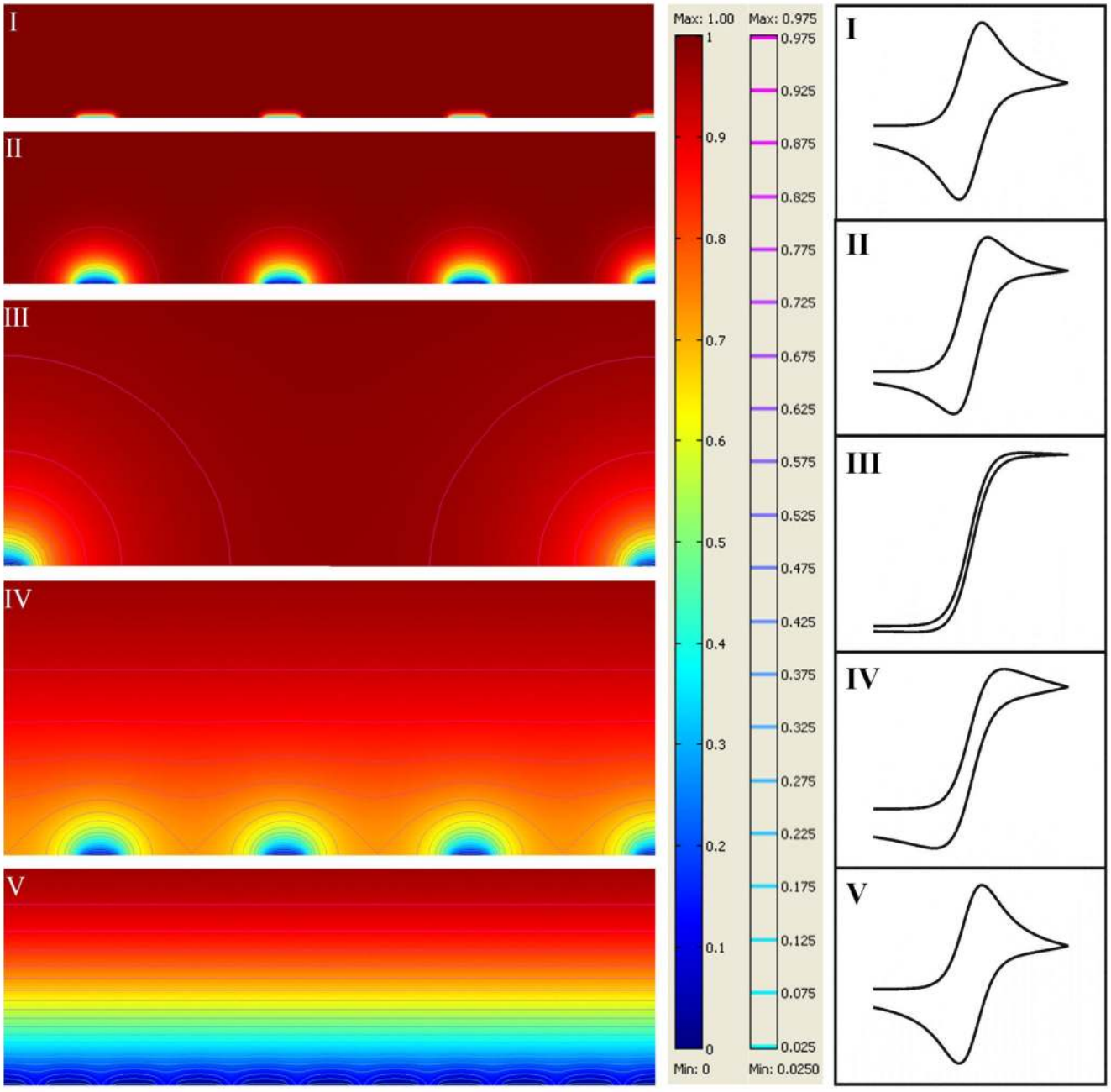

Figure 2.

Simulated concentration profiles with iso-concentration contour lines over a microelectrode array representing the five main categories of diffusion modes: (I) planar diffusion layers on individual microdisc; (II) mixed diffusion layers on individual microdisc; diffusion mode between planar and hemispherical diffusion; (III) hemispherical diffusion layers on individual microdisc; (IV) mixed diffusion layers; diffusion mode of partial overlapping of adjacent diffusion layers; (V) planar diffusion layer over the entire microelectrode array; diffusion mode of complete overlaping of individual diffusion layers. In the scale bar next to the figure the red color represents the bulk concentration and the blue color represents zero concentration. The

second scale bar represents a relative concentration scale for the contour lines. Typical CVs of the each category are shown at the right.

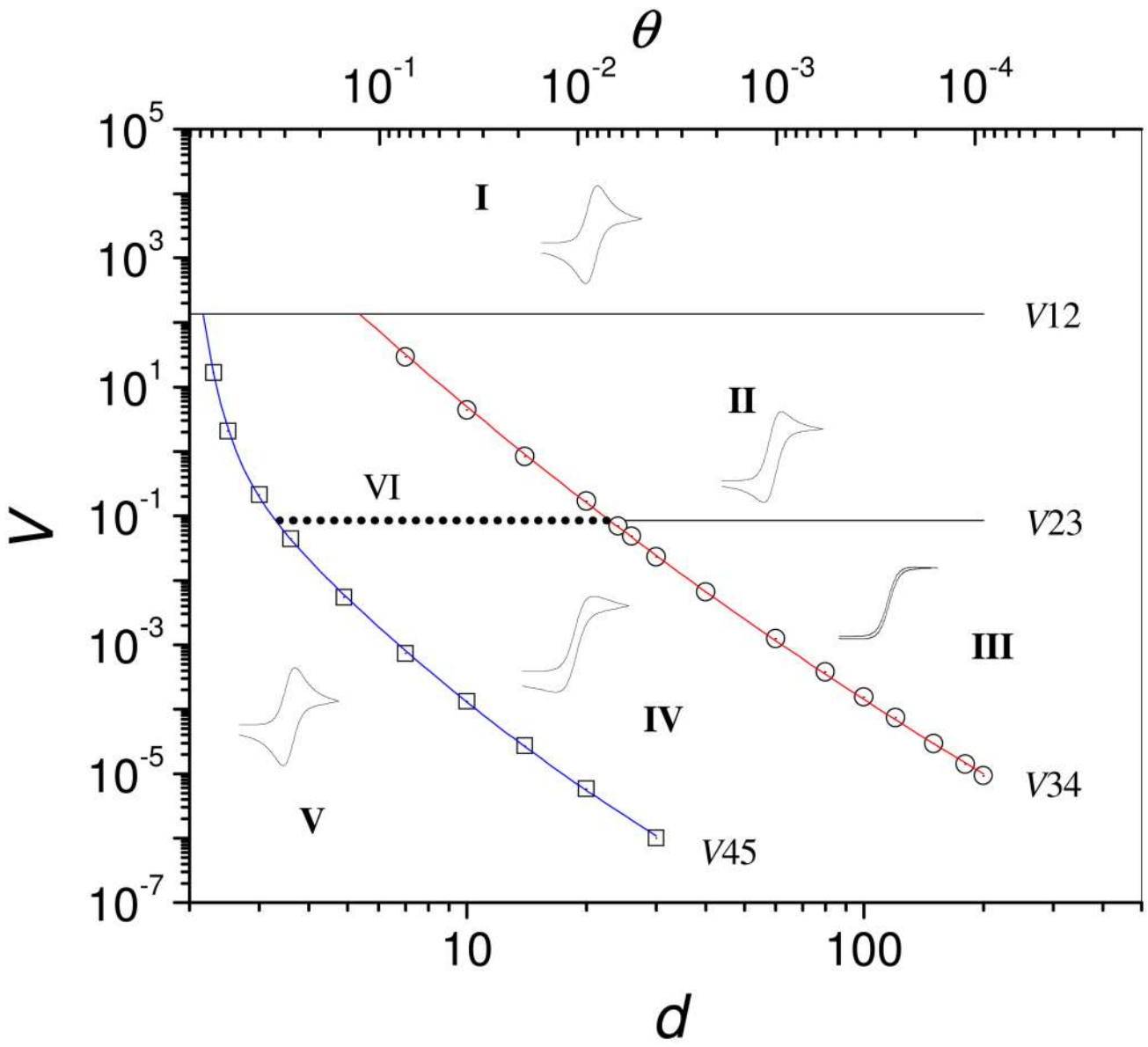

Figure 3.
Zone diagram of cyclic voltammetric behavior at microelectrode arrays. *d* is the center-to center distance of individual electrodes in the array (measured in units of *a*), *V* is the dimensionless scan rate (eq. 4), and θ is the fraction of electrochemically active area in the array.

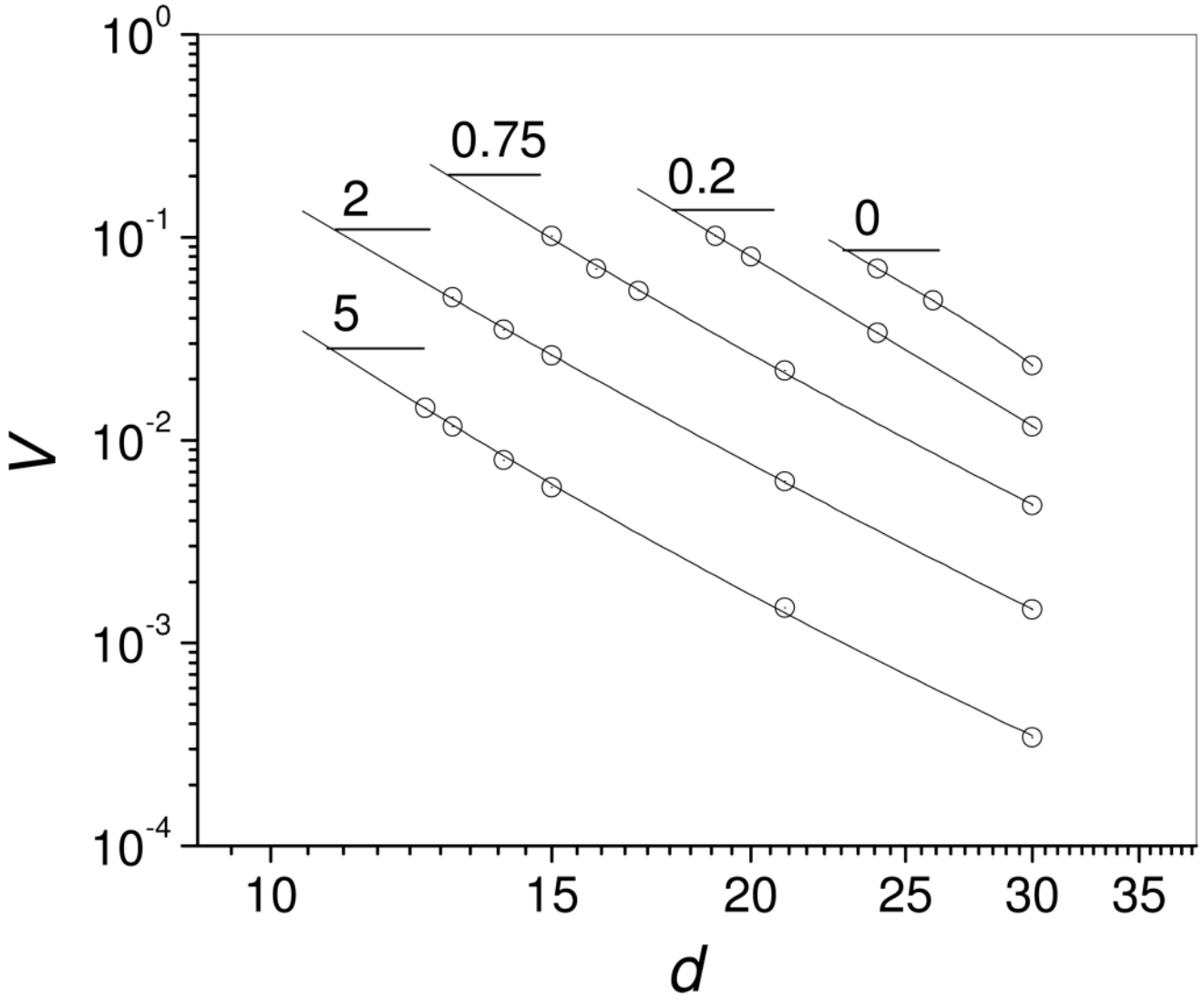

Figure 4.
Enlarged section of the zone diagram (Figure 3) showing the *V*23 and *V*34 line cross sections for shallow recessed microdisc electrode arrays with $L = 0, 0.2, 0.75, 2$ and 5 (numbers labeling the cross sections). Horizontal lines represent *V*23 lines. Slanted lines represent *V*34 lines.

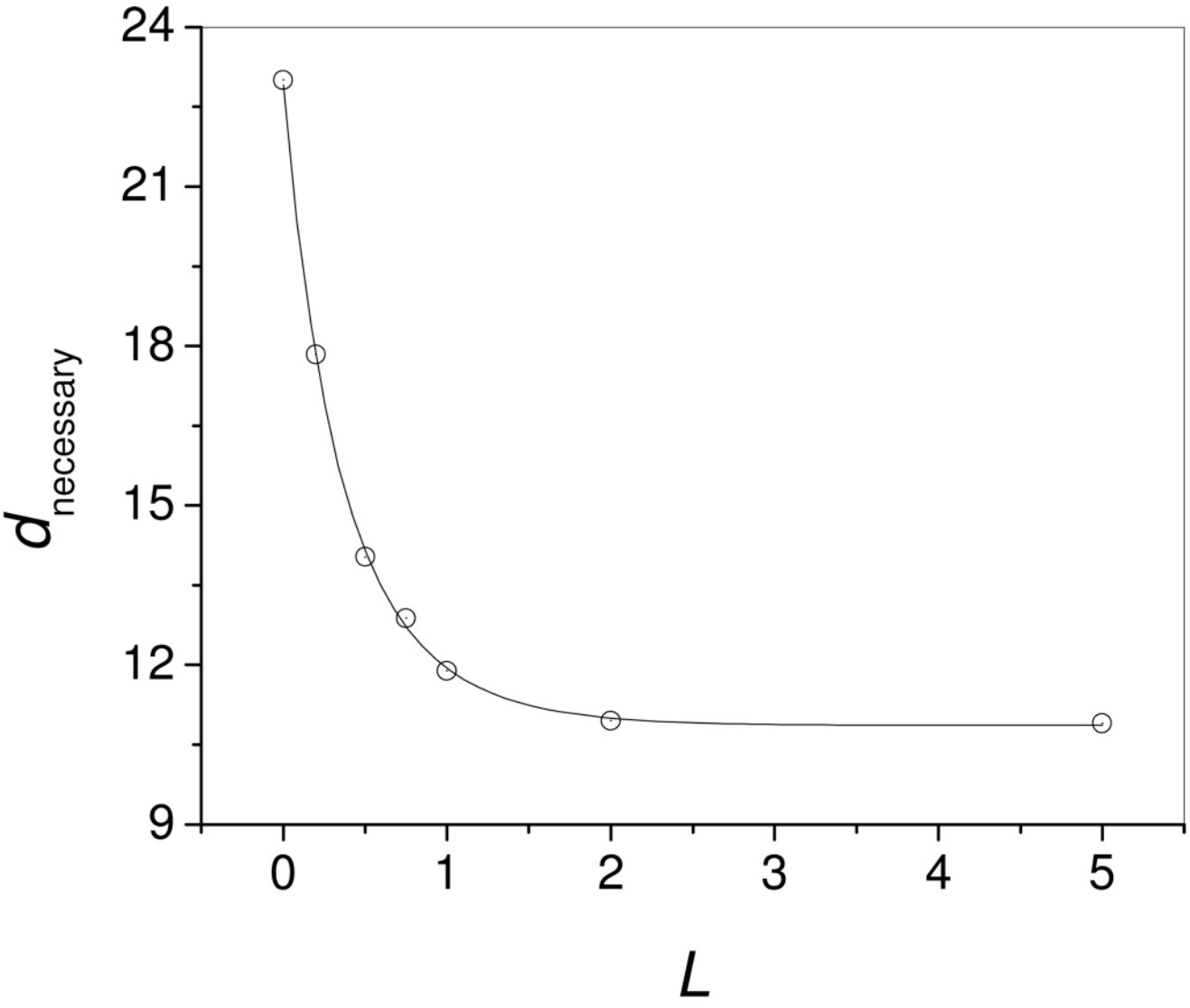

Figure 5.
$d_{necessary}$ (measured in units of a) as function of the dimensionless recess depth (L) for shallow recessed microdisc electrode arrays.

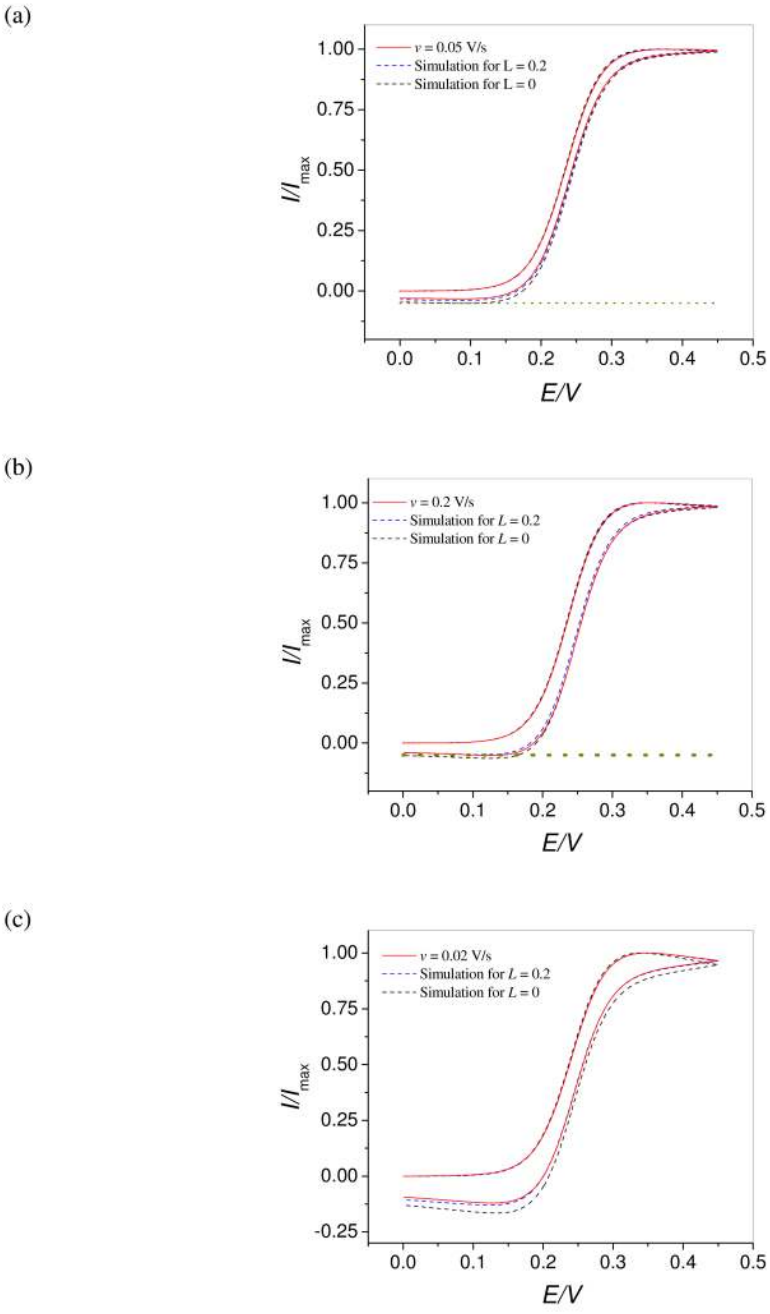

Figure 6.

Comparison of the experimentally recorded CVs at shallow recessed microdisc electrode arrays with simulation results at coplanar and recessed arrays. Experimental data obtained at microelectrode arrays with $a = 5$ μm, $l = 1$ μm, $d = 150$ μm (a) and $d = 100$ μm (b, c) in 1 mM ferrocenemethanol and 0.1 M $NaNO_3$ solution were background-subtracted. Simulations presented with corresponding dimensionless scan rates of 0.01644 (a) 0.06574 (b) and 0.006574 (c) at arrays with $d = 30a$ (a), $d = 20a$ (b, c) and $l = 0.2a$ for recessed. Dotted horizontal lines (dark yellow) in panel a and b indicate 5% increase of γ from baseline.

Table 1

Definition of Dimensionless Transition Scan Rates

Transition Scan Rates	Criterion	
	$I_{max,\ individual}$	$I_{max,\ reverse}/I_{max,\ forward}$ (γ)
*V*12	$I_{max,\ individual} > I_{ss,\ single}$	$\gamma = \gamma_{linear} - 0.05$
*V*23	$I_{max,\ individual} > I_{ss,\ single}$	$\gamma = 0.05$
*V*34	$I_{max,\ individual} < I_{ss,\ single}$	$\gamma = 0.05$ for $d \geq 23.0$
	$I_{max,individual} < I_{max,\ single}$	$\gamma - \gamma_{single} = 0.05$ for $d < 23.0$
*V*45	$I_{max,\ individual} < I_{ss,\ single}$ for $d \geq 3.31$ $I_{max,\ individual} < I_{max,\ single}$ for $d < 3.31$	$\gamma = \gamma_{linear} - 0.05$

Tabel 2

Expressions of Zone Borderlines in Figure 3

Zone borderlines	Expressions
$V12$	136.3
$V23$	0.08562
$\log V34$ ‡	$26.12\exp(-\log d/3.94) - 19.57$
$\log V45$ ‡	$475.8\exp(-\log d/0.0617)+15.73\exp(-\log d/1.87) - 13.11$

‡Equations fitted to simulated points

Table 3

Symbols and acronyms

Symbol	Definition
a	radius of the individual electrodes in the array
c_O and c_R	concentration of the oxidized and reduced species in the solution
c_b	bulk solution concentration
C_O	dimensionless concentration of the oxidized species (Eq. 25)
C_R	dimensionless concentration of the Reduced species (Eq. 26)
d	center-to-center distance between two adjacent microelectrodes in an array; d is measured in units of a.
$d_{necessary}$	Center-to-center distance of two adjacent individual microelectrodes which is large enough to make it possible to record a sigmoidal wave on a MEA. $d_{necessary}$ is measured in units of a.
D	diffusion coefficient
D_O and D_R	diffusion coefficients of the oxidized and reduced species in the solution
E	is the applied potential on the electrode/solution interface
E_i	the initial potential in cyclic voltammetry
E_r	the reversal potential in cyclic voltammetry
$E^{0'}$	is the formal potential
ΔE	potential range in Eq. 3., defined as the potential difference from the foot of the forward wave to the reverse point in a cyclic voltammogram
F	Faraday constant
i	current passing through the individual microelectrode/solution interfaces (Eq. 23 and 24)
$I_{ss,single}$ †	steady state current in the CV obtained on a single microdisc electrode
$I_{max,\ single}$ †	maximum current in the CV obtained on a single microdisc electrode
$I_{max,\ forward}$ †	maximum current for the forward reaction in a CV(e.g. maximum cathodic current)
$I_{max,\ reverse}$ †	maximum current for the reverse reaction in a CV (e.g. maximum anodic current)
$I_{max,\ individual}$ †	maximum current in the CV obtained on individual microdisc electrode in a MEA
k_f	forward rate constants as defined in Eq. 6
k_b	backward rate constant as defined in Eq. 7
k^0	the standard heterogeneous rate constant for the redox couple
K_0	dimensionless rate constant (Eq. 30)
l	recess depth
L	dimensionless recess depth (Eq. 29)
n	the number of electrons transferred in the electrode reaction
O	oxidized species in the solution
r	cylindrical coordinate
R	reduced species in the solution
R	dimensionless r coordinate (Eq. 27)
R	universal gas constant
R_0	radius of a circle equal in area to the individual microelectrode hexagon (Fig. 1a)
t	time
t_c	time scale of the cyclic voltammetric experiment (Eq. 21)
T	thermodynamic temperature

Symbol	Definition
V	dimensionless scan rate (Eq.4)
$V12$	dimensionless transition scan rate borderline between diffusion category I and II in the zone diagram (Fig.3)
$V23$	dimensionless transition scan rate borderline between diffusion category II and III in the zone diagram (Fig.3)
$V34$	dimensionless transition scan rate borderline between the diffusion category III and IV (II and IV in certain domain) in the zone diagram (Fig.3)
$V45$	dimensionless transition scan rate borderline between diffusion category IV and V in the zone diagram (Fig.3)
z	cylindrical coordinate
z_{max}	the maximum z value in the simulation domain
Z	dimensionless z coordinate (Eq.28)
α	transfer coefficient
γ	$\gamma = I_{max,\ reverse}/I_{max,\ forward}$, characterizing the contribution of cottrellian diffusion in a CV
γ_{linear}	γ value calculated from a fully linear diffusion controlled CV
γ_{single}	γ value calculated from a CV obtained on a single microdisc electrode with certain V
ε	dimensionless potential (Eq. 31)
v	potential scan rate
τ	dimensionless time (Eq.32)
θ	fraction of active area in a microelectrode array

† Currents are normalized by the steady state current on a single microdisc electrode